17th World Conference on Earthquake Engineering, 17WCEE
Sendai, Japan - September 13th to 18th 2020

EXPERIMENTAL STUDY OF SELF-CENTERING COMPOSITE SHEAR WALLS WITH CONCEALED STEEL PLATE BRACES

Zhihui Wang(1) , Huidi Yang(2) , Mengfu Wang(3) ,Michael C H Yam(4)

(1) *Ph.D.student, Department of Building & Real Estate, The Hong Kong Polytechnic University, Hong Kong, People's Republic of China, Email: 18045142r@connect.polyu.hk*
(2) *Postgraduate student, College of Civil Engineering, Hunan University, Hunan, People's Republic of China, Email: 2394284001@qq.com*
(3) *Professor, College of Civil Engineering, Hunan University, Hunan, People's Republic of China, Email: wangmengfu@hnu.edu.cn*
(4) *Professor, Department of Building & Real Estate, The Hong Kong Polytechnic University, Hong Kong, People's Republic of China, Email: michael.yam@polyu.edu.hk*

Abstract

Steel-concrete composite shear walls with concealed steel plate braces (SCCSWs) are lateral force-resisting members that are desirable for use in seismic zones for their high lateral strength, deformation capacity and energy dissipating qualities. However, inelastic behavior in the SCCSWs can result in serious damage, large residual drifts and costly repairs in a building after an earthquake. In this paper, two kinds of self-centering SCCSWs are proposed, that is, the self-centering SCCSW with shear steel dowel and energy-dissipation steel bars (SCSCCSW-SR) and the self-centering SCCSW with hinged member (SCSCCSW-H). Furthermore, the self-centering ability of the SCSCCSW-SR and SCSCCSW-H is provided by unbonded prestressed steel tendons inside the wall. Effectiveness of the two proposed walls was investigated by quasi-static tests, and a comparison was made among the traditional SCCSW, the SCSCCSW-SR and the SCSCCSW-H. The experimental results indicated that the average lateral load bearing capacities of specimens SCCSW, SCSCCSW-SR and the SCSCCSW-H was 361.0kN, 340.3kN and 328.2kN respectively; the maximum residual drift ratios of specimens SCCSW, SCSCCSW-SR and SCSCCSW-H was 1.35%, 0.45% and 0.43% respectively; the maximum equivalent viscous damping coefficients of specimens SCCSW, SCSCCSW-SR and SCSCCSW-H was 14.09%, 8.83% and 7.82% respectively; the two proposed wall specimens exhibit excellent self-centering behavior and good energy dissipation ability with the lateral load bearing capacity similar to the traditional SCCSW specimen. From the experimental results, we can find that the cracks and damage of specimen SCSCCSW-SR are mainly concentrated near the wall toes and the cracks and damage of specimen SCSCCSW-H are mainly concentrated near the wall bottom, the crack quantity and damage range in the two proposed wall specimens were significantly reduced compared with the traditional SCCSW. Finally, the analysis methods were developed to calculate load bearing capacity of the two proposed walls, and the computing results agreed well with the measured peak loads.

Keywords: Self-centering; Steel-concrete composite shear wall; Concealed steel plate brace; Prestressed; Quasi-static test.

1. Introduction

Reinforced concrete (RC) shear walls are widely used in high-rise buildings located in seismic regions around the world. To ensure structural safety, RC shear walls must provide sufficient lateral strength, dissipate energy ability and deformation capacity when subjected to maximum considered earthquakes. Recent earthquake reconnaissance reports from the 2010 Chile Maule Earthquake (Mw 8.8) and 2010/2011 New Zealand Christchurch Earthquake (Mw7.1/6.2) [1,2,3] indicated that conventional RC shear walls showed inadequate seismic behaviors, and thousands of conventional RC shear walls were severely damaged and even collapsed. It is necessary to solve the problems existing in conventional RC shear walls located in regions with high seismic intensity.

A lot of experiments and numerical simulations indicated that embedding inclined steel braces [4,5,6] in the RC wall to form the steel-concrete composite shear wall with concealed steel plate braces (SCCSW) could greatly improve seismic performance. The SCCSW showed superiorities in lateral strength, deformation capacity and energy dissipating qualities compared to the traditional RC wall. In the past ten years, The SCCSWs have been used as the primary lateral load-resisting system of buildings in high seismic areas [7,8]. However, when SCCSWs are subjected to severe earthquakes, spalling of concrete and yielding of reinforcement bars mostly are still appeared near the bottom of SCCSWs, and axial-flexural plastic hinge is developed at the bottom of SCCSWs. This can lead to significant residual deformations and costly repairs of the SCCSWs after earthquakes.

To reduce residual drift and damage of structural systems after earthquakes, researchers proposed and studied the purely self-centering RC shear walls, the self-centering hybrid RC shear walls and the self-centering RC coupled wall systems. In the above three self-centering RC shear walls, their self-centering abilities are provided by the unbonded post-tensioned (PT) tendons. The self-centering hybrid RC shear wall is different from the purely self-centering RC shear wall in that various kinds of energy dissipative devices are incorporated into the self-centering hybrid RC shear wall. The self-centering RC coupled wall systems are composed of several purely self-centering RC shear walls and coupling beams or mechanical coupling devices. A lot of experiments and numerical simulations indicated that: the purely self-centering RC shear walls have the smallest residual drift and the most excellent self-centering behavior, but have disadvantages of large drift and small energy dissipation ability [9,10,11,12]; the self-centering hybrid RC shear walls [13,14,15,16,17,18,19] and the self-centering RC coupled wall systems [20,21,23,24,25] exhibit better self-centering behavior and energy dissipation ability.

Based on the research achievements of the SCCSWs and the self-centering hybrid RC shear walls, two kinds of self-centering SCCSWs are proposed, that is, the self-centering SCCSW with shear steel dowel and energy-dissipation steel bars (SCSCCSW-SR) and the self-centering SCCSW with hinged member (SCSCCSW-H). The SCCSW and foundation are connected by the unbonded PT tendons , shear steel dowel and energy-dissipation steel bars to form the SCSCCSW-SR, in which the self-centering ability of the SCSCCSW-SR is provided by unbonded PT tendons inside the wall, the lateral load is mainly resisted by shear steel dowel, and energy dissipation of the SCSCCSW-SR is mainly dependent on the energy-dissipation steel bars which welded with the concealed steel plate braces and fixed in the foundation. The SCCSW and foundation are connected by the unbonded PT tendons and hinged member to form the SCSCCSW-H, in which the self-centering ability of the SCSCCSW-H is also provided by unbonded PT tendons inside the wall, the lateral load and energy dissipation are mainly dependent on the hinged member which welded with the concealed steel plate braces and fixed in the foundation. Effectiveness of the two proposed walls was investigated by quasi-static tests, and a comparison was made among the traditional SCCSW, the SCSCCSW-SR and the SCSCCSW-H. Meanwhile, the analysis methods were developed to calculate load bearing capacity of the two proposed walls.

2. Experimental Program

2.1 General information of specimen

Three specimens including one traditional SCCSW, one SCSCCSW-SR and one SCSCCSW-H (Table 1) were constructed and tested under quasi-static cyclic loadings. The geometrical dimensions of the three specimens were identical. the length, the height and the thickness of wall piers were 1000mm,1450mm and 160mm respectively. the horizontal load was applied at 1625mm high above the foundation interface, and the aspect ratio (AR) is 1.625. The rocking response of the specimens can be achieved according to ACI ITG-5.1[26], in which the AR of 0.5 is recommended. Fig.1 depict the reinforcement and steel bracing details of the tested specimens for different arrangement with elevation and cross section (SCCSW, SCSCCSW-SR, SCSCCSW-H) respectively. Steel strands with a diameter of 15.2mm were used in the prestressed elements of the two proposed wall specimens, and the unbonded length of the steel strands are equivalent to the total height of test specimens. In terms of ACI ITG-5.2[26], the choice initial prestressing values of the two proposed wall specimens is 430MPa. Separating steel plates in the two proposed wall specimens were placed at the bottom of wall and welded with the vertical reinforcements and steel bracings of wall. The axial load applied on all three specimens was $0.1A_g f_c$ (f_c: the design value of axial compressive strength of concrete; A_g: cross-sectional area of the wall), and the design axial load ratio of all three specimens is 0.1.

In specimen SCSCCSW-SR, to resist any slide at the wall-foundation interface, one shear dowel made of steel was used and placed across the middle position at the base of the specimen. To enhance energy dissipation ability of the self-centering walls, the two energy-dissipation steel bars were used in the specimen and welded with the concealed steel plate braces and fixed in the foundation. In specimen SCSCCSW-H, the hinged member was placed near the middle position at the top of foundation beam and with anchor bars embedded in the foundation beam. Meanwhile, the hinged member and the concealed steel plate braces were welded by steel bars.

Table 1 – Main parameters of the tested wall specimens

Specimen	wall pier		boundary zone		shear steel dowel	hinged member	quantity of steel strands
	Horizontal	Vertical	Longit	Transv.e			
SCCSW	Ø10@200	Ø10@150	4Ø12	Ø6 @120	-	-	-
SCSCCSW-SR	Ø10@200	Ø10@150	4Ø12	Ø6 @120	1Ø60	-	2Ø15.2
SCSCCSW-H	Ø10@200	Ø10@150	4Ø12	Ø6 @120	-	1	2Ø15.2

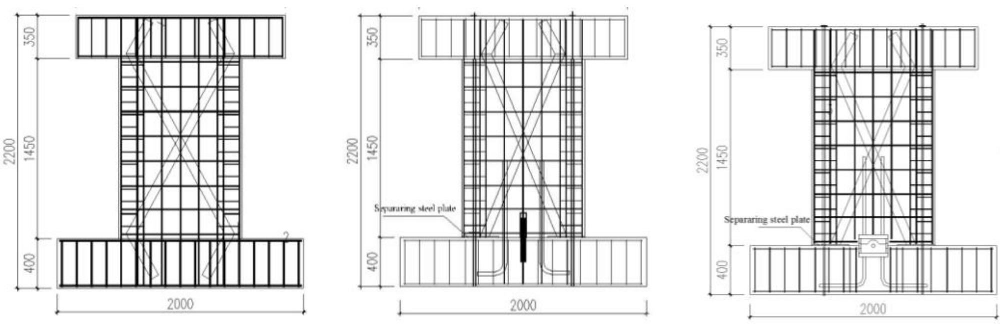

(a) (b) (c)

Fig. 1–Configuration details of specimens(elevation): (a) SCCSW; (b) SCSCCSW-SR; (c) SCSCCSW-H

2.2 Construction methodology

During the construction of specimens SCSCCSW-SR and SCSCCSW-H, the steel strands, shear steel dowel or hinged member and the joint-crossing energy-dissipation steel bars were placed vertically in their design position and were cast together in the foundation beam. Then the reinforcing bars and concealed steel plate braces in wall piers, the reinforcing bars in loading beams and the separate steel plates were assembled before casting concrete (Fig.2). After casting concrete, the steel strands were prestressed to the design level (F_T=78kN). There were no obvious construction differences between the traditional cast-in-place specimen SCCSW and the prestressed specimens SCSCCSW-SR, SCSCCSW-H.

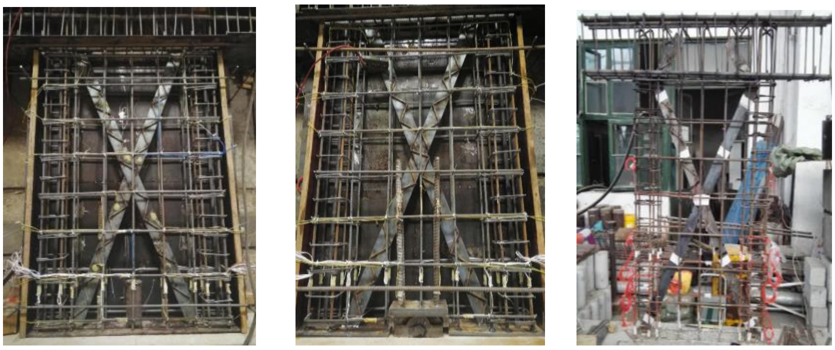

(a) (b) (c)

Fig. 2 – Specimens during construction: (a) SCSCCSW-SR; (b) SCSCCSW-H; (c) SCCSW

2.3 Test setup and procedure

A schematic representation of test setup are shown in Fig.3a. Two triangle steel truss structures were used to prevent wall pier deformations in the out-of-plane directions. A constant vertical load F_N of 230kN was applied by hydraulic jack at the top of the specimens, and design axial load ratios of the specimens are 0.1. The specimens were subjected to the horizontal force from an actuator connected to the reaction column. The loading was controlled by the top horizontal displacement or top horizontal drift angle, the loading program is shown in Fig.3b. the test is ended when the horizontal loading displacements are larger than the certain lateral load displacements.

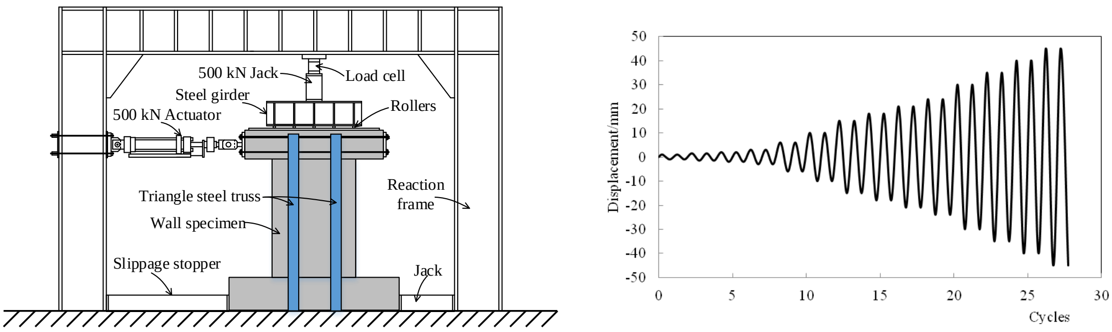

(a) (b)

Fig.3 – Test setup and cyclic loading history: (a) test setup; (b) cyclic loading history of test

2.4 Material properties

Self-Compacting Concrete (SCC) used for casting all specimens was prepared in the laboratory and designed as a nominal cubic compressive strength $f_{cu,d}$ of 30MPa. The designed mix proportions of SCC are shown in Table 2. The principal components of concrete as follows: (1) typical normal Portland cement with a nominal compressive strength of 42.5 MPa as the binder for mixtures, (2) normal river sand with fineness modulus of 2.4 as the fine aggregates, (3) river gravel with sizes between 5 and 20mm as the coarse aggregates, (4) ordinary tap water, (5) a highly efficient polycarboxylate-based superplasticizer, (6) fly ash at a grade of 1. According to the requirement of Chinese technical specification (JGJT283-2012) [27], workability of SCC was evaluated with slump-flow tests. The slump flow diameter is 705 mm in average, and the slump flow time is 1.8s. Concrete samples were kept in cubes of 150 mm×150mm×150mm size when concrete was pouring. The actual cubic compressive strength of these samples was tested before the experimental test at an age of 28 days. The measured average concrete compressive strength f_{cu} of specimens SCCSW , SCSCCSW-SR and SCSCCSW-H were 37.8 MPa, 33.5MPa and 33.5MPa, respectively.

Ø6 rebars were HPB300 Grade plain rebars (nominal yield strength f_y = 300MPa) while other rebars were HRB400 Grade deformed bars (f_y = 400MPa). Steel plate bracings were Q235 Grade (f_y = 210MPa). The material properties of reinforcement, steel plate and steel strand were measured by coupon tests, and test values of yield and ultimate strength are summarized in Table 3.

Table 2 – Mix proportion of SCC (kg/m^3)

Cement	Water	Fly ash	Fine aggregate	Coarse aggregate	Superplasticizer
317	180	168	810	843	5.4

Table 3 – Material properties of reinforcement, steel plate and steel strand

Type	Diameter/ steel thickness	Yield strength f_y (N/mm^2)	Ultimate strength f_u (N/mm^2)
Deformed bar	Ø6	437	493
	Ø10	489	583
	Ø12	462	591
Steel strand	Ø15.2	1763	1940
Steel bracing	t5	262	421

3.Test result and discussion

3.1 General observations

Specimen SCCSW was a cast-in-place steel-concrete composite shear walls with concealed steel plate braces, and its energy dissipation was finished through the formation of a plastic hinge at the bottom of the wall pier. An initial crack occurred horizontally 200mm~220mm distant from the bottom of the wall pier at the load of 145kN, and then an oblique crack appeared when the lateral displacement increased to 15mm. The load bearing capacity of specimen SCCSW was achieved at 21mm load step. The crushing of concrete at the wall toes and was observed and cracks was developed through the bottom of the wall at the lateral displacement of 30mm, Fig.4a shows the concrete crack distribution and failure patterns after the test of specimen SCCSW.

Specimen SCSCCSW-SR was in elastic stage and no crack was occurred when the lateral displacement is smaller 1.5mm. Horizontal cracks were initiated at the lateral displacement of 2mm and appeared at 50mm distant from the bottom of the wall pier. When the lateral displacement was increased to 10mm, concrete cracks were developed along the horizontal direction of wall bottom. With the increase of lateral displacement, the quantity and width of horizonal cracks were increased, but crack development was focused near the wall toes. Vertical cracks of wall toes were observed and concrete cover spalling was occurred at the 35mm load step, almost no oblique crack was appeared. The load bearing capacity of specimen SCSCCSW-SR was achieved at 40mm load step, and obvious concrete spalling can be observed. Test of specimen SCSCCSW-SR ended after the cycle of 45mm, and the concrete of wall toes was crushed and the maximum concrete crack area of wall toes is 100mm×120mm in this load case. Fig.4b shows the concrete crack distribution and failure patterns after the test of specimen SCSCCSW-SR. The gap opening and closing of specimens can be clearly observed during the test, the maximum opening height of specimen SCSCCSW-SR is about 20mm.

Specimen SCSCCSW-H was also in elastic stage and no crack was occurred when the lateral displacement is smaller 1.5mm. Horizontal cracks were initiated at the lateral displacement of 2mm and appeared near the wall toes. When the lateral displacement was increased to 10mm, a horizontal crack with length of 50mm was appeared at one side of the hinged member. With the increase of lateral displacement, the quantity and width of horizonal cracks at the two sides of the hinged member were increased. Horizontal through cracks between wall toes and hinged member were formed at the 35mm load step, almost no oblique crack was appeared. The load bearing capacity of specimen SCSCCSW-SR was achieved at 40mm load step, and obvious concrete spalling can be observed. Test of specimen SCSCCSW-R ended after the cycle of 45mm, and the concrete of wall toes was crushed. Fig.4c shows the concrete crack distribution and failure patterns after the test of specimen SCSCCSW-H. The gap opening and closing of specimens can be clearly observed during the test, but the maximum opening height of specimen SCSCCSW-H is smaller than that of SCSCCSW-SR.

Obviously, specimen SCCSW showed typical flexural-shear failure pattern. Specimen SCSCCSW-SR and specimen SCSCCSW-H showed the flexural damage pattern with few oblique cracks, and the failure of specimens SCSCCSW-SR and SCSCCSW-H was the results of the crushing of the concrete at the wall toes.

(a) (b) (c)

Fig. 4 – Failure patterns of specimens: (a) SCCSW; (b) SCSCCSW-SR; (c) SCSCCSW-H

3.2 Hysteretic curves

The lateral force versus top displacement hysteretic curves for the three tested specimens are depicted in Fig. 5a, b, c. The hysteretic curve shape of traditional self-centering RC shear walls is close each other; the typical hysteretic curve of the traditional self-centering RC shear wall specimen PM6 is shown in Fig.5d [28].

Some observations can be made from Fig.5. Firstly, the three tested specimens have almost the same the initial stiffness. With the increase of lateral displacement, the stiffness degradations in specimen SCSCCSW-SR and specimen SCSCCSW-H were lower than that of specimen SCCSW, which plays a favorable role in preventing the collapse of SCSCCSW-SR and SCSCCSW-H under rare earthquakes. Secondly, the characteristics of hysteretic curves for specimen SCSCCSW-SR and specimen SCSCCSW-H were similar, the areas of the hysteresis loops for specimen SCSCCSW-SR and specimen SCSCCSW-H are little less than that of specimen SCCSW; since hysteresis loops of the traditional self-centering RC shear wall specimen PM6 shown in Fig.5d are extremely narrow, the areas of the hysteresis loops for specimen SCSCCSW-SR and specimen SCSCCSW-H are much larger than that of the traditional self-centering RC shear wall. The comparisons indicate that SCSCCSW-SR and SCSCCSW-H have much better energy dissipation ability than the traditional self-centering RC shear wall. Finally, the residual drifts of specimen SCSCCSW-SR and specimen SCSCCSW-H were much smaller than that of specimen SCCSW. The comparisons indicate that SCSCCSW-SR and SCSCCSW-H performed better than SCCSW, and showed good self-centering ability.

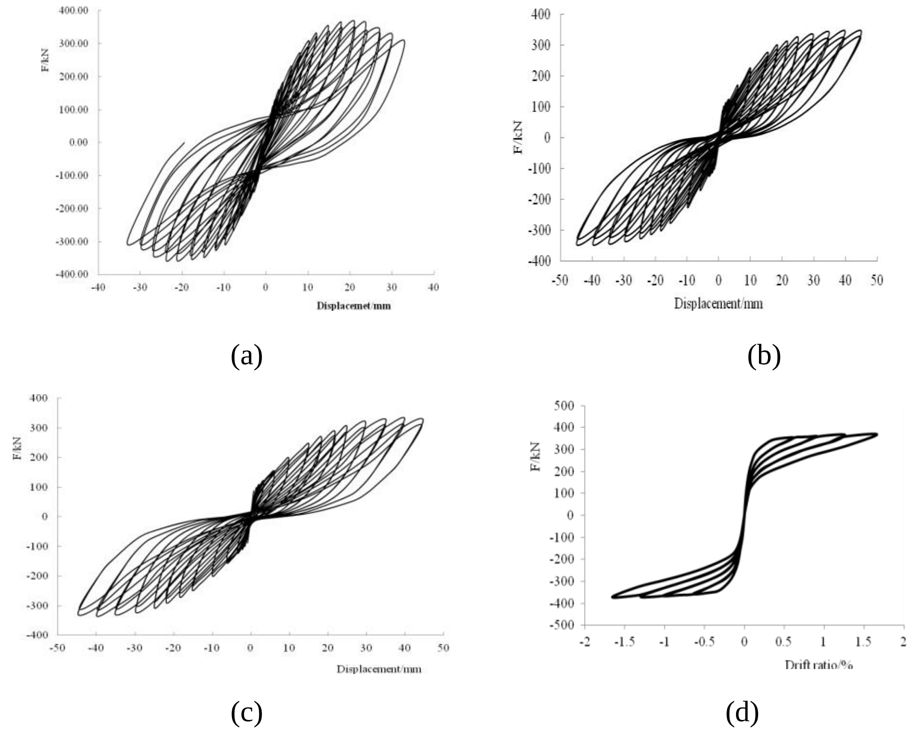

Fig. 5 – Hysteretic curves of specimens: (a) SCCSW; (b) SCSCCSW-SR; (c) SCSCCSW-H; (d) PM6

3.3 Backbone curves

The backbone curves of the three specimens in this paper were compared shown in Fig.6. At 40mm displacement (top drift ratio=2.46%), specimen SCSCCSW-SR and specimen SCSCCSW-H reached their maximum strength while that of specimen SCCSW occurred at loading displacement 20mm (top drift ratio=1.23%). The average lateral load bearing capacities of specimens SCCSW， SCSCCSW-SR and SCSCCSW-H were 361.0kN, 340.3k11N and 328.2kN respectively; Compared with specimen SCCSW, the average maximum strength of specimens SCSCCSW-SR and SCSCCSW-H were dropped by 5.7% and 9.1%, respectively. The lateral load bearing capacities of specimens SCSCCSW-SR and SCSCCSW-H were similar to the traditional specimen SCCSW. Besides, the ultimate lateral displacement of specimen SCCSW was equivalent to 33mm, and was far less than that of specimens SCSCCSW-SR and SCSCCSW-H.

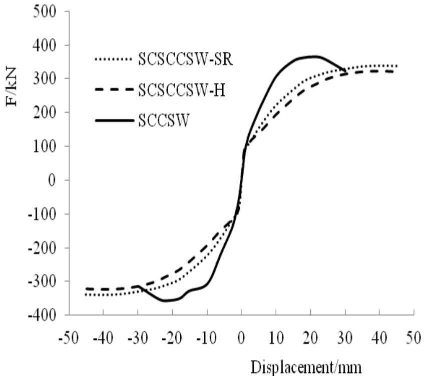

Fig. 6 – Backbone curves of the specimens

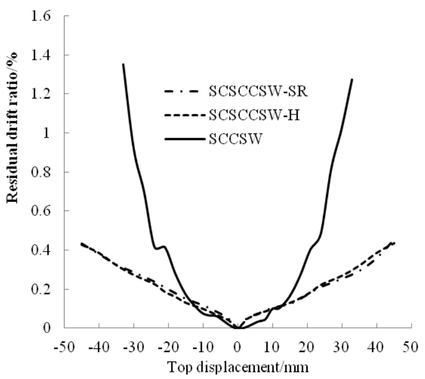

Fig.7 – Residual drifts of the specimens

3.4 Residual drift

The residual drifts at the first cycle of each load step are plotted in Fig. 7. It shows that after loading step of 15mm, specimens SCSCCSW-SR and SCSCCSW-H performed as expected with much less residual drift on unloading when compared to specimen SCCSW. The maximum residual drift ratios of specimens SCCSW, SCSCCSW-SR and SCSCCSW-H were 1.35%, 0.45% and 0.43% respectively. The acceptable maximum residual drift of 0.5% was recommended by Rahman and Sritharan [29] at the maximum drift ratio of 2.5%. Therefore, the residual drifts of specimens SCSCCSW-SR and SCSCCSW-H were all acceptable according to Fig. 7. The results indicate that the self-centering ability was achieved by placing separating steel plates and steel strands.

3.5 Energy dissipation

The equivalent viscous damping coefficient ζ_{eq} was defined as follows

$$\zeta_{eq} = \frac{E_D}{2\pi E_s} \tag{1}$$

where E_D represents the dissipation energy at each loading cycle, E_S represent the elastic strain energy at each loading cycle. The equivalent viscous damping coefficients of specimens SCCSW, SCSCCSW-SR and SCSCCSW-H at each loading cycle are plotted in Fig.8.

As demonstrated in Fig.8, the equivalent viscous damping coefficients of specimens SCCSW, SCSCCSW-SR and SCSCCSW-H are close to each other before loading displacement 10mm. However, the equivalent damping coefficients of specimen SCCSW gradually exceeded that of specimens SCSCCSW-SR and SCSCCSW-H after loading displacement 15mm. The maximum equivalent viscous damping coefficients of specimens SCCSW, SCSCCSW-SR and SCSCCSW-H were 14.0%, 8.8% and 7.8% respectively.

For comparison, the equivalent viscous damping coefficients of the traditional self-centering RC shear wall specimen PM6 was computed by using equation (1). The equivalent viscous damping coefficients of specimen PM6 are from 2.2% to 2.7%.

From the above analysis results, we found that the SCCSW has the highest equivalent viscous damping coefficient value, the SCSCCSW-SR and the SCSCCSW-H have higher equivalent viscous damping coefficient values, the equivalent viscous damping coefficients of the traditional self-centering RC shear wall were far less than that of specimens SCSCCSW-SR and SCSCCSW-H.

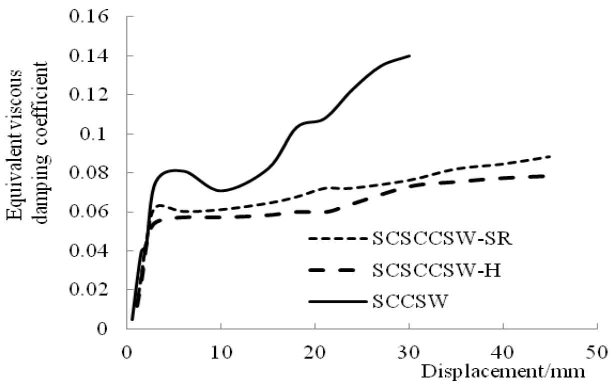

Fig.8 – The equivalent viscous damping coefficients of specimens

4. Load bearing capacity of the two proposed walls

4.1 Basic assumptions

In order to calculate the normal section loading capacity of the two proposed walls, the following assumptions are made based on the experimental results of specimens SCSCCSW-SR and SCSCCSW-H:

(1). Displacements are distributed linearly across the tension zone of wall panel, the validation-level roof drift in ACI ITG-5.1[26] is taken as the ultimate rotate angle θ_u of wall panel:

$$\theta_u = 0.008\frac{H_w}{L_w} + 0.005 \tag{2}$$

Where H_w is the height of wall and L_w is the length of wall.

(2) Strains are distributed linearly across the compression zone of wall panel; the ultimate compressive strain ε_u is to be taken as 0,0033[30];

(3) The rebars are elastic before yielding, and maintain a yield stress after yielding;

(4) A rectangular equivalent stress block is introduced for the concrete compressive stress distribution, equivalent stress block parameters for concrete compressive zone (α and β) follow the recommendation of GB 50011-2010 [30]. When concrete strength grade is not more than C50, α =1.0, β = 0.8; when concrete strength grade is C80, α =0.94, β = 0.74; Intermediate values are obtained by linear interpolation.

(5) If the steel bracing and some rebars in the concrete compression zone are not yielded, the contribution of the steel bracing and these rebars to load bearing capacity of specimens are ignored [31].

4.2 Load bearing capacity of the SCSCCSW-SR

Based on gap opening at base joint of specimen SCSCCSW-SR shown in Fig.9 and the above assumptions, the related parameters are described as

$$\delta_P = (0.5L_w + a_2 - c_u)\theta_u,\ \varepsilon_{pc} = (c_u - 0.5L_w + a_2)\varepsilon_u / c_u \tag{3}$$

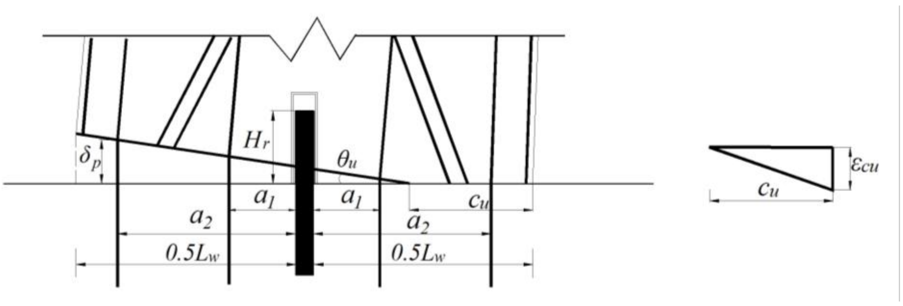

Fig.9 – Gap opening at base joint of specimen SCSCCSW-SR

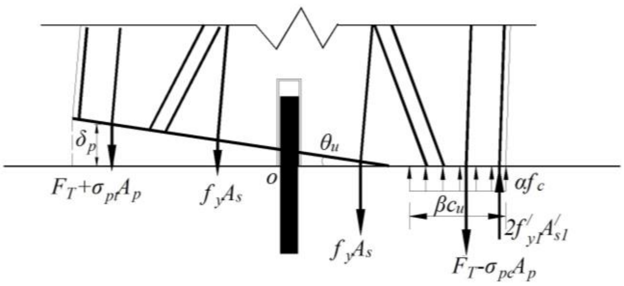

Fig.10 – Simplified free body diagram of base joint of specimen SCSCCSW-SR

Based on the mechanical model shown in Fig.10 and applying the equilibrium conditions, we obtain

$$2F_T + N_P + 2f_y A_s + \sigma_{pt} A_p - \sigma_{pc} A_p - \alpha\beta b c_u f_c - 2f'_{y1} A'_{s1} = 0 \quad (4)$$

and the moment resistance of the cross section about the point O:

$$M_u = (\sigma_{pt} + \sigma_{pc}) A_p a_2 + 0.5\alpha\beta b c_u f_c (L_w - \beta c_u) + 2f'_{y1} A'_{s1} (0.5L_w - a) + H_r F_u = H_w F_u \quad (5)$$

where

$$\sigma_{pt} = E_p \delta_p / H_p,\ \sigma_{pc} = E_p \varepsilon_{pc},\ f_c = 0.67 f_{cu},\ A_p = \pi d_p^2 / 4,\ A_s = \pi d_s^2 / 4,\ A'_{s1} = \pi d_{s1}^2 / 4 \quad (6)$$

In which,

$$E_p = 1.95\times10^5\,\text{MPa},\ f_y = f'_{y1} = 462\,\text{MPa},\ f_{cu} = 33.5\,\text{MPa},\ d_s = 25\text{mm},\ d_{s1} = 12\text{mm}$$

$$d_p = 15.2\text{mm},\ L_w = 1000\text{mm},\ H_w = 1625\text{mm},\ H_p = 2200\text{mm},\ H_r = 200\text{mm},\ a = 21\text{mm} \quad (7)$$

Substituting the above parameters into equation (4), (5), we can obtain

$$c_u = 290.6\text{mm},\ F_u = 330.4\ \text{kN},\ M_u = 536.88\ \text{kN}\cdot\text{m} \quad (8)$$

The calculated value F_u=330.4kN of load bearing capacity for specimen SCSCCSW-SR is 2.9% less than the test value F_u=340.3kN, the calculated value is in good agreement with the test result and more conservative.

4.3 Load bearing capacity of the SCSCCSW-H

Based on gap opening at base joint of specimen SCSCCSW-H shown in Fig.11 and the above assumptions, the related parameters are described as

$$\delta_P = a_2\theta_u,\ \varepsilon_{pc} = (a_2 - a_1)\varepsilon_u / c_u,\ c_u = 0.5L_w - a_1 \quad (9)$$

Based on the mechanical model shown in Fig.11 and applying the equilibrium conditions, we obtain the moment resistance of the cross section about the point O:

$$M_u = (\sigma_{pt} + \sigma_{pc}) A_p a_2 + 0.5\alpha\beta b c_u f_c (L_w - \beta c_u) + 2f'_{y1} A'_{s1} (0.5L_w - a) = H_w F_u \quad (10)$$

where

$$\sigma_{pt} = E_p \varepsilon_{pt} = E_p \delta_p / H_p,\ \sigma_{pc} = E_p \varepsilon_{pc},\ f_c = 0.67 f_{cu} \quad (11)$$

Substituting the related parameters in equation (7) into equation (10), we can obtain

$$F_u = 314.3\ \text{kN},\ M_u = 510.71\ \text{kN}\cdot\text{m} \quad (12)$$

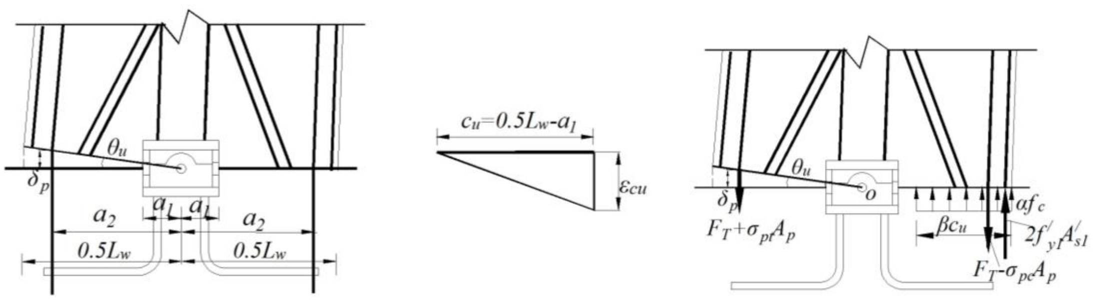

Fig.11 – Gap opening and simplified free body diagram of base joint of specimen SCSCCSW-H

The calculated value F_u=314.3kN of load bearing capacity for specimen SCSCCSW-H is 4.2% less than the test value F_u=328.2kN, the calculated value is in good agreement with the test result and more conservative.

5. Conclusion

In this paper, cyclic loading tests of one traditional SCCSW, one SCSCCSW-SR and one SCSCCSW-H were performed, the computing formulae of load bearing capacity of the SCSCCSW-SR and the SCSCCSW-H were developed. The results of the study are summarized as follows:

(1). The average lateral load bearing capacities of specimens SCCSW， SCSCCSW-SR and SCSCCSW-H were 361.0kN, 340.3kN and 328.2kN respectively; Compared with specimen SCCSW, the average maximum strength of specimens SCSCCSW-SR and SCSCCSW-H were dropped by 5.7% and 9.1%, respectively. The lateral load bearing capacities of specimens SCSCCSW-SR and SCSCCSW-H were similar to the traditional specimen SCCSW.

(2). The maximum residual drift ratios of specimens SCCSW，SCSCCSW-SR and SCSCCSW-H was 1.35%, 0.45% and 0.43% respectively; the maximum equivalent viscous damping coefficients of specimens SCCSW，SCSCCSW-SR and SCSCCSW-H was 14.09%, 8.83% and 7.82% respectively; the proposed SCSCCSW-SR and SCSCCSW-H exhibit excellent self-centering behavior and good energy dissipation ability with the lateral load bearing capacity similar to the traditional SCCSW specimen.

(3). The cracks and damage of SCSCCSW-SR are mainly concentrated near the wall toes and the cracks and damage of specimen SCSCCSW-H are mainly concentrated near the wall bottom, the crack quantity and damage range in the proposed SCSCCSW-SR and SCSCCSW-H were significantly reduced compared with the traditional SCCSW.

(4). The mechanical models were developed to estimate the load bearing capacity of the proposed SCSCCSW-SR and SCSCCSW-H. The calculated values of the proposed SCSCCSW-SR and SCSCCSW-H agree well with the measured peak loads with errors less than 4.2%, and the calculated results are conservative to the measured peak load.

6. References

[1] EERI (2010). The Mw 8.8 Chile earthquake of February 27, 2010. EERI Earthquake Special Report.

[2] Kam WY, Pampanin S, Dhakal RP, Gavin HP, Roeder CW (2010): Seismic Performance of Reinforced Concrete Buildings in the 4th September 2010 Darfield (Canterbury) Earthquake. Bulletin of the New Zealand Society for Earthquake Engineering, 43(4), 340–350.

[3] Kam WY, Pampanin S (2011): The seismic performance of RC buildings in the 22 February 2011 Christchurch earthquake. Structural Concrete, 12, 223–233.

[4] Cao WL, Xue SD, Zhang JW (2003). Seismic performance of RC shear walls with concealed bracing. Advance in Structural Engineering, 6, 1–13.

[5] Wang MF, Song XY, Wang ZH (2013). Experimental study on seismic performance of high damping concrete shear wall with concealed bracings. Earthquake Engineering and Engineering Vibration, 33(5), 153–161. (in Chinese)

[6] Lan WW, Ma JX, Li B (2015). Seismic performance of steel-concrete composite structural walls with internal bracings. Journal of Constructional Steel Research, 110, 76–89.

[7] Jiang HJ, Fu B, Liu LE, Yin XW (2014). Study on seismic performance of a super-tall steel-concrete hybrid structure. Structural Design of Tall and Special Buildings, 23, 334–349.

[8] Ji XD, Leong TS, Qian JR, Qi WH, Yang WB (2016). Cyclic shear behavior of composite walls with encased steel braces. Engineering Structures, 127, 117–128.

[9] Kurama YC, Sause R, Pessiki S, et al (1997). Seismic design and response evaluation of unbonded post-tensioned precast concrete walls. No.EQ-97-01, Department of Civil and Environmental Engineering, Lehigh University.

[10] Erkmen B, Schultz AE (2009). Self-centering behavior of unbonded post-tensioned precast concrete shear walls. Journal of Earthquake Engineering, 13 (7), 1047 - 1064.

[11] Perez FJ, Sause R, Pessiki S (2007). Analytical and experimental Lateral load behavior of unbonded posttensioned precast concrete walls. Journal of Structural Engineering, 133(11), 1531 - 1540.

[12] Perez FJ, Pessiki S, Sause R (2013). Experimental lateral load response of unbonded post-tensioned precast concrete walls. ACI Structural Journal, 110 (6), 1047 - 1055.

[13] Restrepo J, Rahman A (2007). Seismic performance of self-centering structural walls incorporating energy dissipaters. Journal of Structural Engineering, 133 (11), 1560 -1570.

[14] Holden T, Restrepo J, John B. et al (2003). Seismic performance of Precast reinforced and prestressed concrete walls. Journal of Structural Engineering, 129 (3), 286 - 296.

[15] Smith BJ, Kurama YC, et al (2011). Design and measured behavior of a hybrid precast concrete wall specimen for seismic regions. Journal of Structural Engineering, 137 (10), 1052-1062.

[16] Smith BJ, Kurama YC, McGinnis MJ, et al (2013). Behavior of Precast concrete shear walls for seismic regions: comparison of hybrid and emulative specimens. Journal of Structural Engineering, 139 (11), 1917 - 1927.

[17] Marriott D, Pampanin S, Bull D, et al (2008). Dynamic testing of precast, post-tensioned rocking wall systems with alternative dissipating solutions. Bulletin of the New Zealand Society for Earthquake Engineering, 41(2), 90 - 103.

[18] Lu XL, Dang XL, Qian J, et al (2016). Experimental study of self-centering shear walls with horizontal bottom slits, Journal of Structural Engineering 2016: 04016183.

[19] Gu AQ, Zhou Y, Li QU, et al (2019). experimental study and parameter analysis on the seismic performance of self-centering hybrid reinforced concrete shear walls. Soil Dynamics and Earthquake Engineering, 116, 409-420.

[20] Nakaki SD, Stanton JF, Sritharan S (1999). An Overview of the PRESSS Five-Story Precast Test Building. PCI Journal, 44(2), 26- 39.

[21] Priestley MJN, Sritharan S, Conley JR, Pampanin SS (1999). Preliminary Results and Conclusions From the PRESSS Five-Story Precast Concrete Test Building .PCI Journal, 44(6), 42-67.

[22] Henry RS, Aaleti S, Sritharan S (2010). Concept and finite-element modeling of new steel shear connectors for self-centering wall systems. Journal of Structural Engineering, 136 (2), 220 - 229.

[23] Sritharan S, Aaleti S, Henry RS (2015). Precast concrete wall with end columns (PreWEC) for earthquake resistant design. Earthquake Engineering and Structural Dynamics, 44, 2075–2092.

[24] Henry RS, Sritharan S, Ingham J (2016). Finite element analysis of the PreWEC self-centering concrete wall system. Engineering Structures, 115, 28-41.

[25] Guo T, Zhang GD, Chen C (2013). Experimental study on self-centering concrete wall with distributed friction devices. Journal of Earthquake Engineering, 18 (2), 214 - 230.

[26] ACI (American Concrete Institute) (2009). Requirements for design of a special unbonded post-tensioned precast structural walls satisfying ACI ITG-5.1. ACI ITG5.2-09, Farmington Hills, MI.

[27] JGJT 283-2012 (2012). Technical specification for application of self-compacting concrete. Beijing: China Architecture & Building Press.

[28] Kurama YC, Sause R, Pessiki S, et al (1999). Lateral load behavior and seismic design of unbonded post-tensioned precast concrete walls. ACI Structural Journal, 96(4), 622-632.

[29] Rahman A, Sritharan S (2007). Performance-based seismic evaluation of two five-story precast concrete hybrid frame buildings. Journal of Structural Engineering, 133 (11), 1489-1500.

[30] GB50010-2010 (2015). Code for design of concrete structures. China Architecture and Building Press.

[31] JGJ 3-2010 (2010). Technical specification for concrete structures of tall building. China Architecture & Building Press Beijing, China.

